Computer Three-Dimensional Reconstruction of the Sinoatrial Node

H. Dobrzynski, PhD*; J. Li, PhD*; J. Tellez, BSc; I.D. Greener, BSc; V.P. Nikolski, PhD; S.E. Wright, MD; S.H. Parson, PhD; S.A. Jones, PhD; M.K. Lancaster, PhD; M. Yamamoto, MD; H. Honjo, MD; Y. Takagishi, PhD; I. Kodama, MD; I.R. Efimov, PhD; R. Billeter, PhD; M.R. Boyett, PhD

Background—There is an effort to build an anatomically and biophysically detailed virtual heart, and, although there are models for the atria and ventricles, there is no model for the sinoatrial node (SAN). For the SAN to show pacemaking and drive atrial muscle, theoretically, there should be a gradient in electrical coupling from the center to the periphery of the SAN and an interdigitation of SAN and atrial cells at the periphery. Any model should include such features.

Methods and Results—Staining of rabbit SAN preparations for histology, middle neurofilament, atrial natriuretic peptide, and connexin (Cx) 43 revealed multiple cell types within and around the SAN (SAN and atrial cells, fibroblasts, and adipocytes). In contrast to atrial cells, all SAN cells expressed middle neurofilament (but not atrial natriuretic peptide) mRNA and protein. However, 2 distinct SAN cell types were observed: cells in the center (leading pacemaker site) were small, were organized in a mesh, and did not express Cx43. In contrast, cells in the periphery (exit pathway from the SAN) were large, were arranged predominantly in parallel, often expressed Cx43, and were mixed with atrial cells. An ≈2.5-million-element array model of the SAN and surrounding atrium, incorporating all cell types, was constructed.

Conclusions—For the first time, a 3D anatomically detailed mathematical model of the SAN has been constructed, and this shows the presence of a specialized interface between the SAN and atrial muscle. (***Circulation*. 2005;111:846-854.**)

Key Words: sinoatrial node ■ pacemakers ■ imaging, three-dimensional ■ models, theoretical ■ computer simulation

Theoretically, it is difficult for the sinoatrial node (SAN), a relatively small tissue, to show pacemaker activity and drive the surrounding large mass of more hyperpolarized atrial muscle, because the atrial muscle can electronically hyperpolarize the SAN and suppress pacemaking.[1] Theoretically, this can be prevented by the cells in the SAN center being poorly electrically coupled.[1] Indeed, the 90- and 160-pS conductance connexin isoforms, Cx43 and Cx40, which are abundant in atrial muscle, are either absent or poorly expressed in the SAN center, and the 30-pS isoform, Cx45, is expressed instead.[2–5] However, if electrical coupling were uniformly poor throughout the SAN, the SAN would be unable to drive atrial muscle, and therefore, it has been postulated that in the SAN periphery (at the junction of SAN with atrial muscle), there should be strong electrical coupling.[1] In this study, we have mapped in detail the distribution of SAN cells in the right atrium using SAN-specific markers: middle (160/165-kDa) neurofilament (NF-M) and atrial natriuretic peptide (ANP). NF-M is a neuronal cytoskeletal protein that in the rabbit is expressed exclusively in the cardiac conduction system[6–8] and has previously been used as a marker of rabbit SAN and atrioventricular node cells.[4,9,10] ANP is well known to be abundantly expressed in atrial muscle and not in the SAN.[11,12] We have obtained evidence of the postulated strong electrical coupling (Cx43 expression) in the SAN periphery. To aid the functioning of the SAN, it has also been suggested that there are interdigitating bundles of SAN and atrial cells at the border between the two.[3,13] An alternative but related suggestion is that the whole of the SAN is made up of a mosaic of SAN and atrial cells and that the proportion of the 2 cell types varies from the center to the periphery of the SAN ("mosaic" model).[10] In the present study, we observed an intermingling of SAN and atrial cells in the SAN periphery, although no atrial cells were observed in the SAN center. There is an effort to build an anatomically and biophysically detailed mathematical model of the whole heart,[14] and we present here the first such model of the SAN.

Methods

Methods are described in the online Data Supplement. Experiments were performed on the SAN of New Zealand White rabbits (electrophysiology, n>10; histology, n=6; immunohistochemistry, n=7; RNA isolation, n=7). All data shown are typical.

Results

Identification of Different Cell Types in the SAN

Figure 1A shows a SAN preparation in which the activation sequence was mapped using fluorescent imaging with

Received August 18, 2004; revision received September 13, 2004; accepted September 29, 2004.

From the University of Leeds, Leeds, UK (H.D., J.L., J.T., I.D.G., S.E.W., S.H.P., S.A.J., M.K.L., M.Y., R.B., M.R.B.); Washington University, St Louis, Mo (V.P.N., I.R.E.); and Nagoya University, Nagoya, Japan (H.H., Y.T., I.K.).

*The first 2 authors contributed equally to this work.

The online-only Data Supplement, which contains supplemental text, figures, and movies about methods used in the study, can be found with this article at http://www.circulationaha.org.

Correspondence to Dr H. Dobrzynski, University of Leeds, Leeds LS2 9JT, UK. E-mail bmshd@leeds.ac.uk

Circulation **is available at http://www.circulationaha.org** **DOI: 10.1161/01.CIR.0000152100.04087.DB**

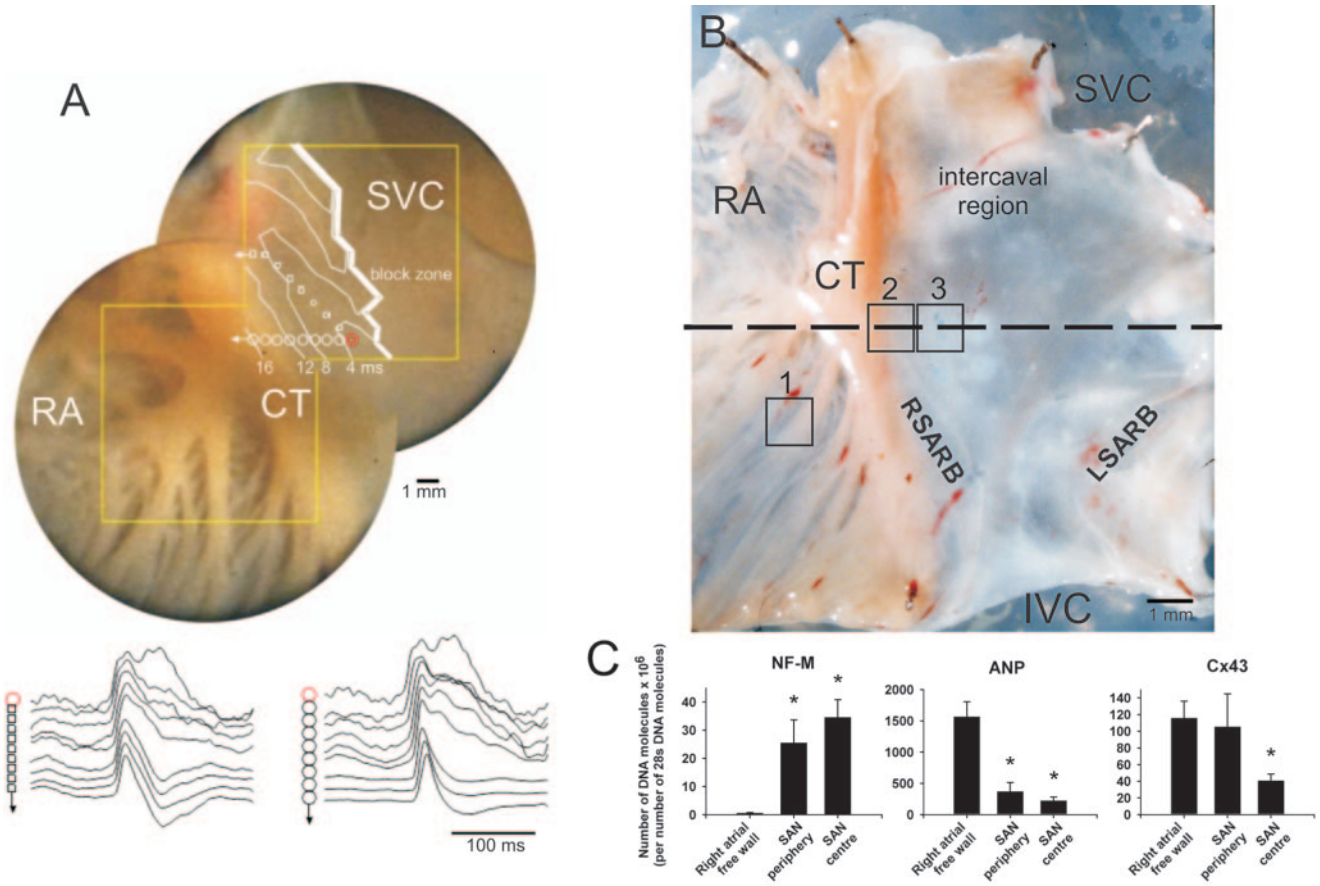

Figure 1. Anatomy, activation pattern, and marker mRNA abundance of tissue under investigation. A (top), Photograph of SAN preparation with activation sequence superimposed (activation time shown by isochrones at 4-ms intervals). Leading pacemaker site is shown by red circle. A (bottom), Optical action potential traces from photodiodes shown by squares and circles in A. Around leading pacemaker site, signal-to-noise ratio is poorer because of thinness of tissue. B, Photograph of SAN preparation showing anatomy, location of samples of right atrial free wall (1) and SAN periphery (2) and center (3) used for C, and approximate line of sections shown in Figure 2. C, Mean (+SEM; n=7) abundance of mRNAs for NF-M, ANP, and Cx43 in right atrial free wall and SAN periphery and center. *Significantly different ($P<0.05$) from right atrial free wall (ANOVA or paired *t* test). IVC indicates inferior vena cava; LSARB, left branch of sinoatrial ring bundle; RA, right atrium; RSARB, right branch of sinoatrial ring bundle; and SVC, superior vena cava.

voltage-sensitive dye (di-4-ANEPPS). The yellow squares show the 16×16 photodiode array mapping areas. Figure 1A also shows optical recordings from 17 different points of the mapped area (symbols in Figure 1A) and shows the initiation and conduction of the action potential. The activation sequence is shown in Figure 1A, and the red circle marks the leading pacemaker site ≈2.6 mm from the border of the crista terminalis (CT) near the main branch of the CT. Data Supplement Movie I shows the activation sequence as an animation. From 4 preparations, sections were cut roughly perpendicular to the CT through the SAN at the expected level of the leading pacemaker site (dashed line in Figure 1B), and they were labeled by immunofluorescence for 2 markers (NF-M and ANP) as well as Cx43. Immunolabeling of neighboring tissue sections is shown in Figure 2. SAN tissue, as identified by NF-M labeling, began in the intercaval region (the region of thin tissue in the rear wall of the right atrium between the superior and inferior venae cavae) and extended from there along the endocardial surface of the CT, where it terminated (Figure 2A; yellow lines mark extent of labeling). ANP labeling was largely a mirror image of NF-M labeling: SAN tissue showing NF-M labeling showed no ANP labeling, whereas atrial muscle showing no NF-M labeling showed ANP labeling (Figure 2). As expected, there was no Cx43 labeling in the SAN center (between red lines in Figure 2C), but there was labeling in atrial muscle (outside yellow lines in Figure 2C). However, Figure 2C shows that there was Cx43 labeling in the SAN periphery (between red and yellow lines in Figure 2C on either side of SAN center). Equivalent data have been obtained from single SAN cells (Data Supplement Figure I).

From 7 rabbits, samples of atrial muscle (right atrial free wall) and SAN periphery and center were collected from the regions shown by the squares in Figure 1B; in the case of SAN periphery, the underlying atrial muscle was removed. The abundance of mRNAs for NF-M, ANP, and Cx43 was measured using real-time polymerase chain reaction and is shown in Figure 1C. Whereas NF-M mRNA was present in the SAN (center and periphery), it was absent from atrial muscle. In contrast, whereas ANP mRNA was abundant in atrial muscle, it was significantly less abundant in the SAN (center and periphery). Cx43 mRNA was abundant in atrial muscle and significantly less abundant in the SAN center. However, in the SAN periphery, the abundance of Cx43 mRNA was the same as in atrial muscle. Expression of proteins and mRNAs is therefore consistent.

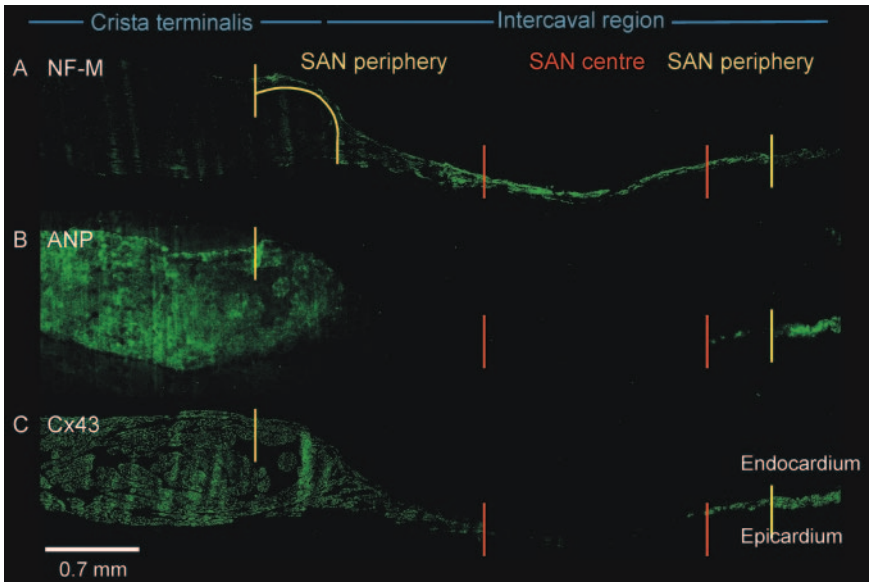

Figure 2. Identification of different cell types in and around SAN by immunofluorescence labeling of NF-M (A), ANP (B), and Cx43 (C) in 3 consecutive sections. Red lines indicate extent of SAN center (Cx43-negative region). Yellow lines indicate extent of SAN (center and periphery) judged by extent of NF-M labeling. SAN periphery lies between red and yellow lines.

Organization of the SAN Periphery

In the remainder of the study, immunoenzyme labeling rather than immunofluorescence labeling was used (because of the ability to identify individual cells), and NF-M was used only as a marker of SAN tissue (anti-ANP was unsuitable for immunoenzyme labeling).

Figure 3, A–D, shows high-magnification images of sections through the CT (atrial muscle) and SAN center (in the intercaval region). The sections were stained with Masson's trichrome; myocytes are stained purple and connective tissue blue. Myocytes in both regions are homogeneous: immunoenzyme labeling showed that all myocytes were either NF-M–negative/Cx43-positive (in CT) or NF-M–positive/Cx43-negative (in SAN center) (data not shown). The sections were cut either parallel or perpendicular to the CT. In the case of the atrial muscle of the CT, the sections cut in different planes are strikingly different (Figure 3A shows atrial cells cut longitudinally, and Figure 3B shows atrial cells cut transversely), whereas in the case of the SAN center, the 2 sections are similar (it is possible to identify cells cut longitudinally or transversely in both sections; Figure 3, C and D). This demonstrates that whereas the atrial cells run longitudinally

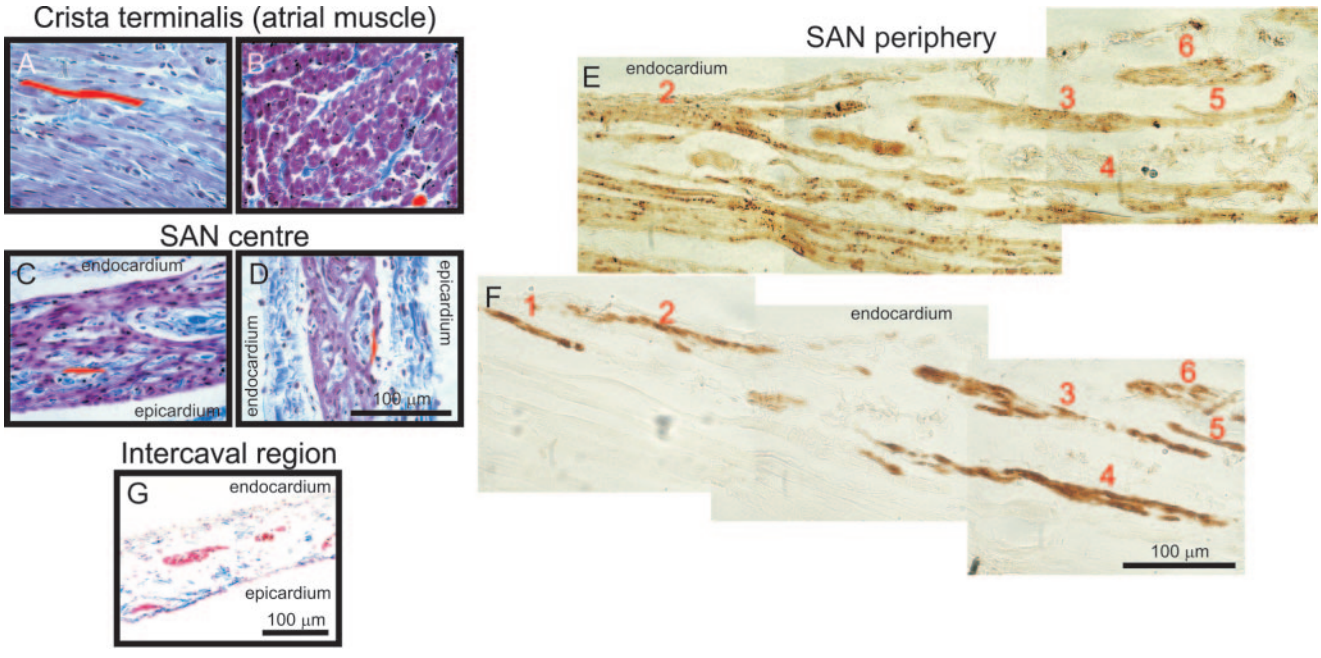

Figure 3. Organization of cells in atrial muscle, in periphery and center of SAN, and in intercaval region toward interatrial septum. A and B, Atrial muscle of CT, cut parallel (A) or perpendicular (B) to CT, stained with Masson's trichrome. C and D, SAN center, cut parallel (C) or perpendicular (D) to CT, stained with Masson's trichrome. E and F, SAN periphery, cut parallel to CT, immunoenzyme-labeled for Cx43 (E) and NF-M (F). In E and F, positive labeling is shown by dark brown color. G, Lack of myocytes in intercaval region. Tissue stained with Masson's trichrome.

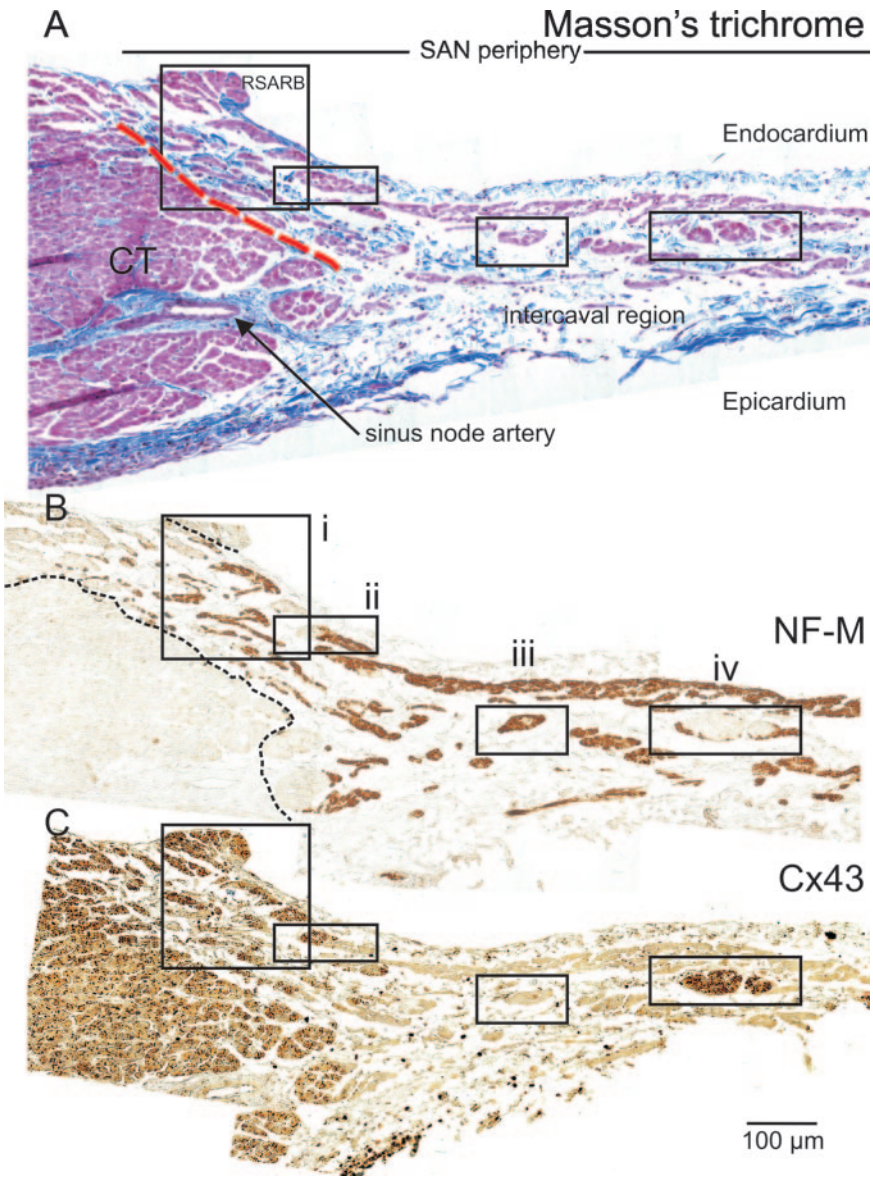

Figure 4. SAN periphery. A–C, Three consecutive tissue sections stained with Masson's trichrome (A) and immunoenzyme-labeled for NF-M (B) and Cx43 (C). In A, red dashed line highlights connective tissue that separates atrial muscle of CT from SAN periphery. In B and C, positive labeling (punctate in C) is shown by dark brown color. Light brown color in C is background.

along the CT, the cells in the SAN center are not uniformly arranged, and they run in different directions to form a mesh. In addition, whereas the atrial cells in the CT are densely packed, the cells in the SAN center are not, and they weave around islands of connective tissue. It is possible to roughly estimate the length and diameter of cells in sections like those in Figure 3, A–D: atrial cells were estimated to be 98±4 and 7±1 μm (n=9), and cells in the SAN center were estimated to be 37±3 and 5±0.2 μm (n=10) in length and width, respectively; example cells are highlighted in Figure 3, A–D.

In contrast to the CT (atrial muscle) and SAN center, the SAN periphery is heterogeneous. Figure 4 shows neighboring sections (cut perpendicular to the CT) through the CT and the intercaval region close to the CT. These sections contain the SAN periphery (at the foot and on the endocardial surface of the CT). They have been stained with Masson's trichrome (Figure 4A) and immunoenzyme-labeled for NF-M (Figure 4B) and Cx43 (Figure 4C). As expected, the sections contain "peripheral" SAN cells that express both NF-M and Cx43 as described above. The region labeled i in Figure 4 is shown at high magnification in Figure 5, A and B, and a similar region from another heart is shown in Figure 5, C and D. Outlined in red are cells expressing both NF-M (Figure 5, A and C) and Cx43 (Figure 5, B and D). Figure 5, E and F, shows the periphery of the SAN on the opposite side of the SAN center (toward the interatrial septum); once again in red are cells expressing both NF-M (Figure 5E) and Cx43 (Figure 5F). However, the periphery of the SAN also contains cells that express NF-M but no or minimal Cx43 (same as central SAN cells, region iii in Figure 4). Furthermore, in the periphery of the SAN there are "atrial cells" (in the tissue shown in Figure 4, 26% of the cells in the periphery, between the dashed lines in Figure 4B, are atrial). An example is region iv at the foot of the CT in Figure 4: the cells in the core of the group express Cx43 but not NF-M (same as atrial cells), whereas the cells on the surface of the group express NF-M but probably not Cx43 (same as central SAN cells). Data Supplement Figure II shows a more extreme example of this arrangement. Another example, on the endocar-

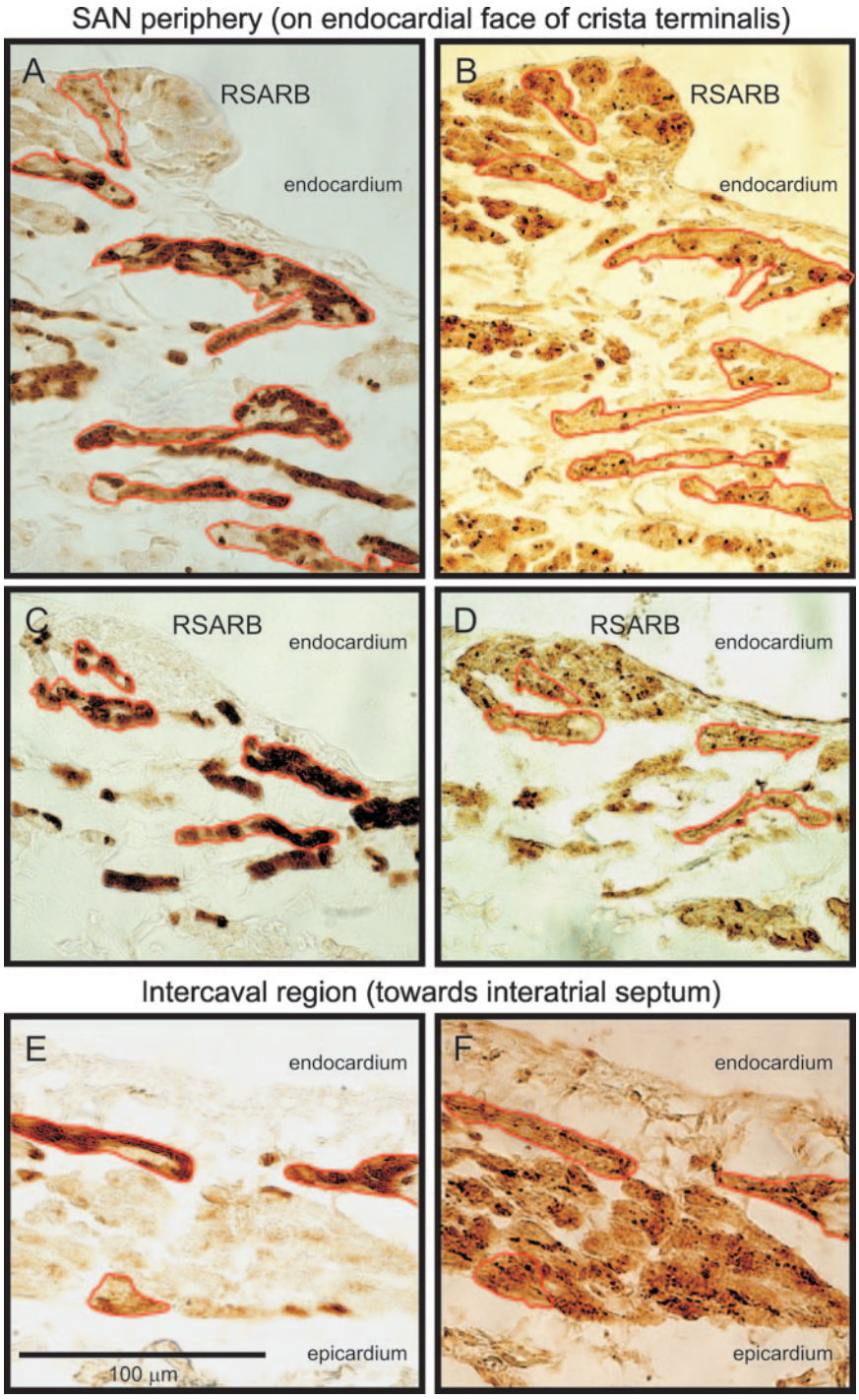

Figure 5. NF-positive and Cx43-positive cells in SAN periphery. A and B, High-magnification views of immunoenzyme labeling of NF-M (A) and Cx43 (B) in tissue next to right sinoatrial ring bundle (from region i in Figure 4). Bundles of NF-positive and Cx43-positive cells are outlined in red. C and D, Similar data from another preparation. E and F, Similar data obtained from intercaval region (toward interatrial septum).

dial surface of the CT, is group ii in Figure 4: the cells on the left of the group express Cx43 but not NF-M (same as atrial cells), whereas the cells on the right express NF-M but not Cx43 (same as central SAN cells). Figure 3, E and F, shows the endocardial surface of adjacent sections through the CT cut parallel to the CT: this is the SAN periphery (where it lies on endocardial surface of the CT). The sections have been immunoenzyme-labeled for Cx43 (Figure 3E) and NF-M (Figure 3F). The majority of the NF-M–positive SAN cells in Figure 3, E and F, are cut longitudinally, and this demonstrates that they run longitudinally along the CT (cell groups 1 to 5 are cut longitudinally, but cell group 6 is cut obliquely). In the periphery, the SAN cells are elongated spindle-shaped cells (Figure 3, E and F) and are unlike the rod-shaped atrial cells of the CT (Figure 3A) or the short spindle-shaped cells of the SAN center (Figure 3C). The approximate length and diameter of cells in the SAN periphery were 86 ± 7 and 8 ± 0.2 μm, respectively ($n=5$).

Images such as that in Figure 4A show that the SAN periphery is broken up into bundles of cells by connective tissue and also that the SAN periphery is separated from the atrial muscle of the CT by connective tissue (red dashed line in Figure 4A). This connective tissue is especially prominent toward the superior vena cava.

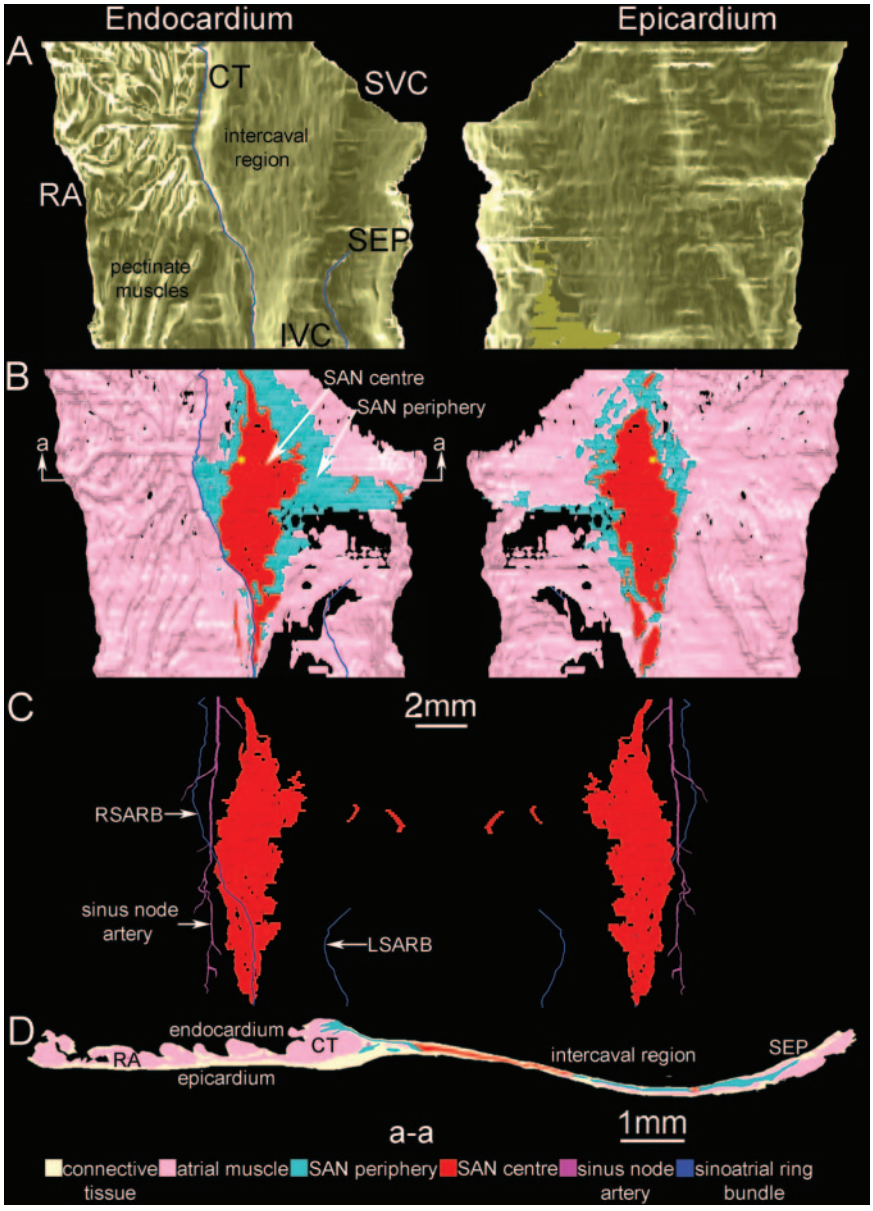

Figure 6. Endocardial (left) and epicardial (right) views of 3D model of SAN. A, Outer surfaces of model. B, Myocytes (outer connective tissue removed). C, SAN center. D, Model section (from line a–a in B). Yellow dot in B marks position of leading pacemaker site. Dark blue line in all panels, sinoatrial ring bundle. SEP indicates interatrial septum.

Absence of Myocytes in the Region of the Block Zone

Figure 1A and Data Supplement Movie I show that, from the leading pacemaker site, conduction occurs toward the CT, and conduction toward the interatrial septum is either slowed or blocked. Figure 3G shows that in the region of the block zone, there is a paucity of myocytes, and this contrasts with the high density of myocytes in the SAN center (Figure 3, C and D). Figure 3G shows islands of myocytes separated by connective tissue. In the region of the block zone, we have also observed a strand of myocytes just one cell thick.

3D Model of SAN

To construct a model, from one preparation, 61 groups of 3 neighboring sections were cut perpendicular to the CT from the top to the bottom of the SAN at ≈200-μm intervals. One section of each group was stained with Masson's trichrome, and the other 2 were immunoenzyme-labeled for NF-M or Cx43. All Masson's trichrome–stained sections are shown in Data Supplement Figure III, and they provided the outline of the tissue and the distribution of myocytes and connective tissue (fibroblasts, adipocytes, collagen fibers). NF-M– and Cx43-immunolabeled sections (eg, Figure 4) were used to divide the myocytes into atrial cells and peripheral and central SAN cells. An example of a model section is shown in Figure 6D: tissue with a majority of NF-M–negative/Cx43-positive myocytes was classified as atrial (pink zone); tissue with a majority of NF-M–positive/Cx43-negative myocytes was classified as central SAN (red zone); tissue with NF-M–positive/Cx43-positive myocytes or a mixture of cell types (NF-M–negative/Cx43-positive and NF-M–positive/Cx43-positive and NF-M–positive/Cx43-negative) was classified as peripheral SAN (blue zone). All model sections are shown in Figure 7. These were used to construct the 3D model of the SAN (see Methods). Figure 6A shows endocardial and epicardial views of the model surface: the endocardial view shows the pectinate muscles, the CT and the smooth interca-

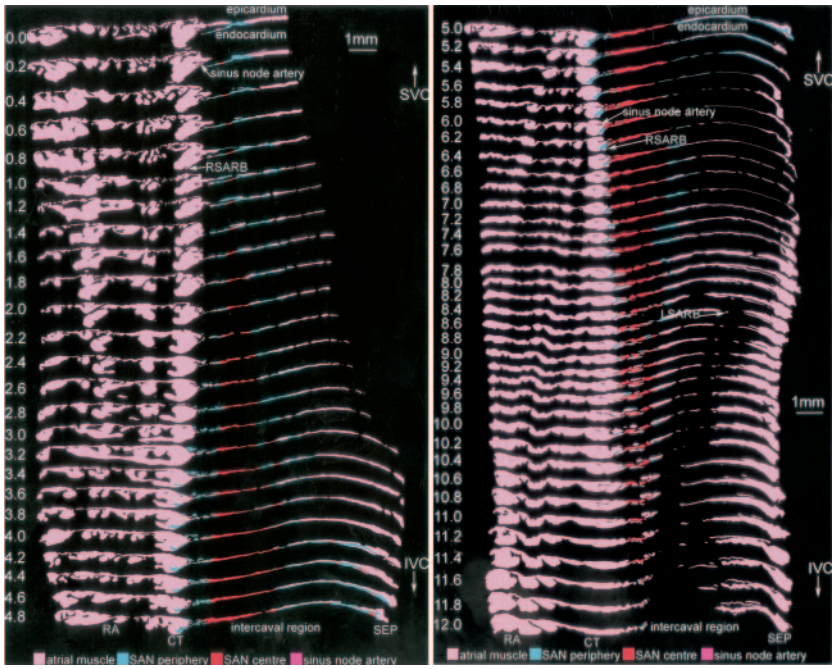

Figure 7. The 61 model sections used to construct 3D model of SAN. Only myocytes are shown (connective tissue not shown). Distance in millimeters from top of preparation shown.

val region, whereas the epicardial view shows the smooth epicardial surface. Figure 6B shows the myocytes below the surface connective tissue. The yellow spot marks the position of the leading pacemaker site (identified by extracellular potential mapping) in this preparation: it lies within the group of central SAN cells (red zone). Figure 6B shows that (1) the SAN tapers superiorly and inferiorly, (2) much of the SAN periphery (blue zone) lies on the endocardial surface of atrial muscle (SAN periphery less evident on the epicardial surface), and (3) there is an absence of myocytes on the septal side and also inferior to the SAN center. Figure 6C shows the central SAN cells only; removal of the other cell types reveals the sinus node artery, a landmark used to locate the SA node. The blue line marks the position of another landmark, the sinoatrial ring bundle. Cell orientation was judged from sections like those in Figure 3, and Figure 8, A and B, shows cell orientation (indicated by lines). Cells ran longitudinally (predominantly) along the CT and the pectinate muscles (Figure 8, A and B). In the SAN periphery, on or adjacent to the CT, many cells ran parallel to the CT (Figure 8, A and B). In a part of the SAN center, cells were oriented in different directions (forming a mesh), and this is indicated by the hatched areas in Figure 8, A and B. The central and peripheral SAN cells occupied volumes of 1.42 and 1.56 mm^3, respectively. The hatched area of the SAN center occupied a volume of 0.37 mm^3. Toward the interatrial septum, cell orientation was varied and complex, but many cells ran perpendicular to the CT. The model shown in Figure 6 corresponds to a typical isolated preparation (such as that in Figure 1B), which has been straightened by being pinned down. To obtain a view of the SAN in situ, an idealized right atrium was generated (white framework in Figure 8C), and the SAN model was "morphed" (see Methods) so that it fitted into the right atrium (Figure 8C). In addition, Figure 8D shows a schematic diagram of the SAN within the heart. Figure 8, C and D, shows that the SAN is extensive and runs alongside the CT from the superior to the inferior vena cava. Movies of the model are available (Data Supplement Movies II and III). The ≈2.5-million-element array model of the anatomy and distribution of cell types is available (Data Supplement File I).

Discussion

The present study has shown the presence of multiple cell types in the SAN. In addition, we have produced a detailed mathematical model of the SAN anatomy incorporating the distribution of the different cell types and cell orientation.

Location of the SAN

The use of NF-M and ANP as markers showed that SAN tissue begins in the intercaval region and extends from here along the endocardial surface of the CT. This corresponds to the distribution of SAN tissue as judged by histology[15] and electrophysiology.[16] The SAN tissue located in the intercaval region is the SAN center; it shows pacemaker activity and is normally the leading pacemaker site.[16] The SAN tissue located on the endocardial surface of the CT is the SAN periphery, and it also shows vigorous pacemaker activity (paradoxically, its intrinsic pacemaker activity is faster than that of the center).[16]

Gradient Versus Mosaic Model

Two models of the organization of the SAN have been proposed.[10,17] According to the gradient model, there are only SAN cells within the SAN, but the SAN cells show a smooth transition in properties (cell size and electrical properties) from the periphery to the center. According to the mosaic model, there are 2 cell types within the SAN (atrial and SAN cells), each with reasonably uniform properties (cell size and electrical properties). According to the mosaic model, the percentage of atrial cells varies from 63% in the periphery to 41% in the center.[10] Figure 4 shows that, contrary to the gradient model and consistent with the mosaic model, there is a mix of atrial and SAN cells in the periphery. However, Figures 2 and 3 show that the cells in the SAN center are small,

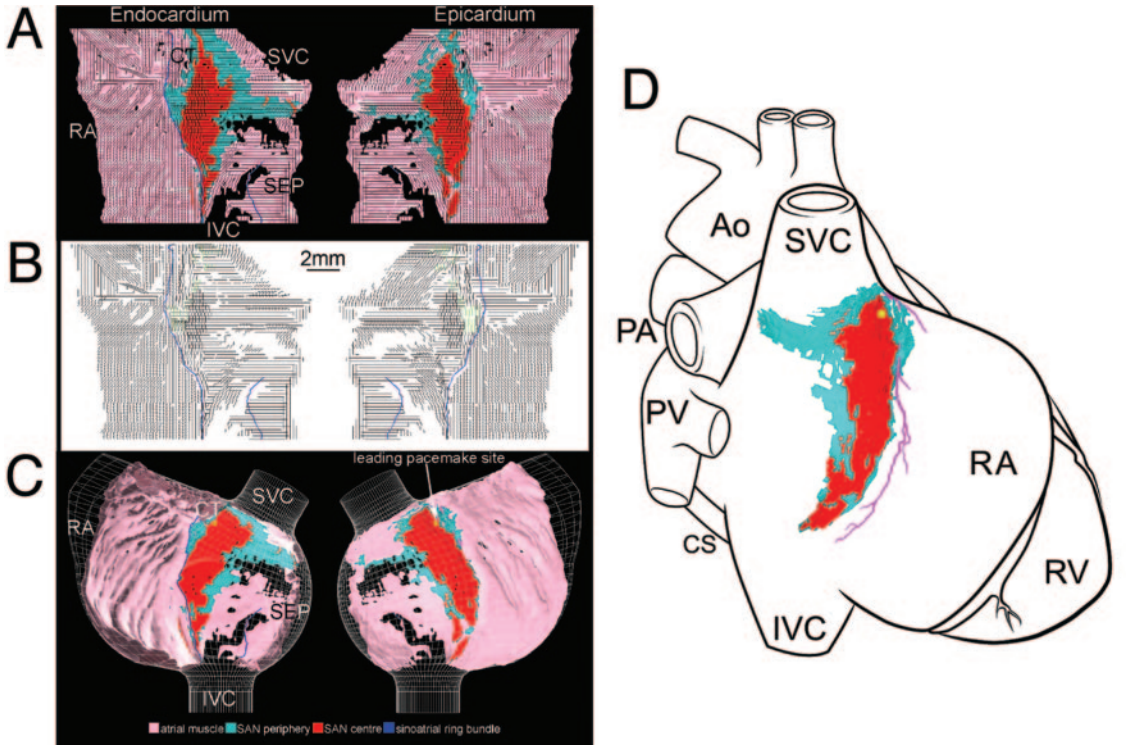

Figure 8. Cell orientation in SAN and location of SAN in heart. A and B, Cell orientation on endocardial (left) and epicardial (right) surfaces superimposed on myocytes (A) and shown alone (B). Black lines, orientation of superficial cells. Green lines, orientation of deeper cells. C, Myocytes of model displayed in a simple framework model of right atrium. D, SAN myocytes displayed on a schematic diagram of heart. Ao indicates aorta; CS, coronary sinus; PA, pulmonary artery; PV, pulmonary vein; and RV, right ventricle.

spindle-shaped, NF-M–positive, ANP-negative, and Cx43-negative; none of these are the attributes of atrial cells, and this is inconsistent with the mosaic model (41% of cells in SAN center should be atrial according to the mosaic model[10]). Therefore, it is possible that elements of both the gradient and mosaic models are correct. This analysis assumes that the functional properties of the cells correlate with the expression of the marker proteins used, but it is possible that this is not the case (these will depend on ion channel expression).

Structure-Function Relationships

The function of the CT is to conduct the action potential from the SAN to the atrioventricular node, and for this the CT is well designed: it consists of atrial cells with little connective tissue, and the atrial cells are large and oriented longitudinally along the length of the CT (Figure 3, A and B) and show abundant expression of high-conductance Cx43 (eg, Figure 2C). The function of the SAN center is different: it is normally the leading pacemaker site. It is composed of a mesh of small SAN cells oriented in different directions wrapped around bundles of connective tissue (Figure 3, C and D). It is interesting to note that we were unable to find tracts of Purkinje-like cells within the SAN, as described by James.[18] Cx43 is not expressed in the SAN center (eg, Figure 2C). It is known that low-conductance Cx45 is expressed in the SAN center instead.[2] The poor electrical coupling in the SAN center provided by Cx45 is important, because it is thought to protect the leading pacemaker site in the SAN from the suppressive influence of the surrounding more hyperpolarized atrial muscle.[1] It is interesting that the pacemaker activity of the atrioventricular node again originates in the small NF-M–positive/Cx43-negative/Cx45-positive nodal cells of the posterior (inferior) nodal extension.[9] To satisfy the conflicting demands of the 2 functions of the SAN (pacemaking and driving atrial muscle), various proposals have been suggested. (1) It has been suggested on theoretical grounds that, although the SAN center should be poorly electrically coupled, the SAN periphery should have better electrical coupling.[1] This study proves that there is such a gradient in electrical coupling from the center to the periphery: whereas in the SAN center, there is no expression of Cx43, in the SAN periphery (identified by NF-M labeling and absence of ANP labeling), Cx43 is expressed (eg, Figure 2C). We have previously shown that Cx43 is expressed in the tissue on the endocardial surface of the CT (but were unable to provide evidence that the tissue was SAN).[2] In addition, we have previously shown that, although Cx43 is not expressed in spider-shaped and spindle-shaped SAN cells (both NF-M–positive and ANP-negative; Data Supplement Figure I), it is expressed in elongated spindle-shaped SAN cells (again NF-M–positive and ANP-negative; Data Supplement Figure I).[19] This is consistent with the present study, because small cells (spider-shaped and spindle-shaped cells) are likely to be from the center, and large cells (elongated spindle-shaped cells) are likely to be from the periphery. Evidence of a gradient in electrical coupling has also been reported in the dog.[5] (2) In various species (including humans), interdigitations of atrial and SAN cells have been reported, and on theoretical grounds, it has

been suggested that these interdigitations permit the SAN to drive the surrounding atrial muscle and at the same time be protected from the hyperpolarizing influence of the atrial muscle.[3,4,10,13] In the present study, we did observe an intermingling of bundles of atrial and SAN cells in the SAN periphery (Figure 4). In the SAN periphery, the cells are divided into bundles, and, in sections perpendicular to the CT, there appears to be no continuous pathway from the SAN center to the atrial muscle (Figure 4). However, conduction is continuous in the periphery of the SAN (Figure 1A), and therefore, the bundles presumably coalesce and divide, thus providing a continuous but tortuous pathway. This feature may also help to isolate the SAN center from the hyperpolarizing influence of the atrial muscle. It may also help to explain why, within the SAN, the conduction velocity is greater parallel to the CT than perpendicular to it (Figure 1A; see also Reference 17). It is interesting that on the septal side of the SAN center, there was also a mixing of SAN and atrial cells: there were overlapping layers of atrial and peripheral SAN (NF-M–positive/Cx43-positive) cells (Figure 6D).

Block Zone

Between the leading pacemaker site in the SAN center and the interatrial septum, a block zone has been observed in various species (eg, Figure 1A).[17] The present study shows that the block may be simply explained by an absence or a reduced number of myocytes in this zone (Figure 6B). However, the absence of conduction in this zone could also be the result of a reduced excitability of the myocytes.[20]

SAN Model

There is an effort to build a virtual heart,[14] and this is the first 3D anatomically detailed mathematical model of the SAN. A virtual heart will be important for research, teaching, and drug development. For example, the SAN is conventionally considered to be located at the base of the superior vena cava,[18] and yet Figure 8, C and D, shows that the SAN is extensive and extends from the superior to the inferior vena cava. This, however, is consistent with the apparent location of the leading pacemaker site in the human and other species[21,22] and the phenomenon of pacemaker shift.[17] Furthermore, in the human, in addition to the body of the SAN at the base of the superior vena cava, the SAN has a long tail that projects toward the inferior vena cava within the CT[23]; this is equivalent to the organization in the rabbit. In the future, we will use the anatomically detailed model to simulate the electrical activity of the SAN. Using the same methods, we have just completed a 3D anatomically detailed model of the atrioventricular node.

Limitations of the Study

The 3D anatomically detailed mathematical model of the SAN was based on one heart only (the construction of one model required 18 months); therefore, no account was taken of interindividual variation (although the essential features of the model were confirmed in other preparations). The model shows the general distribution of cell types. However, the red zone (SAN center) in Figures 6 to 8 includes myocytes and fibroblasts, and the blue zone (SAN periphery) in Figures 6 to 8 includes multiple cell types, and it was not possible to incorporate the distribution of the different cell types within the red and blue zones. The functioning of the SAN depends on ion channels, and in the future, the distribution of ion channels should be incorporated into the model.

References

1. Joyner RW, van Capelle FJL. Propagation through electrically coupled cells: how a small SA node drives a large atrium. *Biophys J*. 1986;50:1157–1164.
2. Coppen SR, Kodama I, Boyett MR, Dobrzynski H, Takagishi Y, Honjo H, Yeh H-I, Severs NJ. Connexin45, a major connexin of the rabbit sinoatrial node, is co-expressed with connexin43 in a restricted zone at the nodal-crista terminalis border. *J Histochem Cytochem*. 1999;47:907–918.
3. Oosthoek PW, Viragh S, Mayen AEM, van Kempen MJA, Lamers WH, Moorman AFM. Immunohistochemical delineation of the conduction system, I: the sinoatrial node. *Circ Res*. 1993;73:473–481.
4. Verheule S, van Kempen MJ, Postma S, Rook MB, Jongsma HJ. Gap junctions in the rabbit sinoatrial node. *Am J Physiol*. 2001;280: H2103–H2115.
5. Kwong KF, Schuessler RB, Green KG, Laing JG, Beyer EC, Boineau JP, Saffitz JE. Differential expression of gap junction proteins in the canine sinus node. *Circ Res*. 1998;82:604–612.
6. Gorza L, Vitadello M. Distribution of conduction system fibers in the developing and adult rabbit heart revealed by an antineurofilament antibody. *Circ Res*. 1989;65:360–369.
7. Gorza L, Schiaffino S, Vitadello M. Heart conduction system: a neural crest derivative? *Brain Res*. 1988;457:360–366.
8. Vitadello M, Vettore S, Lamar E, Chien KR, Gorza L. Neurofilament M mRNA is expressed in conduction system myocytes of the developing and adult rabbit heart. *J Mol Cell Cardiol*. 1996;28:1833–1844.
9. Dobrzynski H, Nikolski VP, Sambelashvili AT, Greener ID, Boyett MR, Efimov IR. Site of origin and molecular substrate of atrioventricular junctional rhythm in the rabbit heart. *Circ Res*. 2003;93:1102–1110.
10. Verheijck EE, Wessels A, van Ginneken ACG, Bourier J, Markman MWM, Vermeulen JLM, de Bakker JMT, Lamers WH, Opthof T, Bouman LN. Distribution of atrial and nodal cells within rabbit sinoatrial node: models of sinoatrial transition. *Circulation*. 1998;97:1623–1631.
11. Sola C, Thibault G, Haile-Meskel H, Anand-Srivastava MB, Garcia R, Cantin M. Atrial natriuretic factor in the vena cava and sinus node. *J Histochem Cytochem*. 1990;38:1123–1135.
12. Benvenuti LA, Aiello VD, Higuchi ML, Palomino SA. Immunohistochemical expression of atrial natriuretic peptide (ANP) in the conducting system and internodal atrial myocardium of human hearts. *Acta Histochem*. 1997;99:187–193.
13. Winslow RL, Jongsma HJ. Role of tissue geometry and spatial localization of gap junctions in generation of the pacemaker potential. *J Physiol.* 1995;487:126P.
14. Hunter PJ, Kohl P, Noble D. Integrative models of the heart: achievements and limitations. *Phil Trans R Soc Lond A*. 2001;359:1049–1054.
15. Bleeker WK, Mackaay AJC, Masson-Pévet M, Bouman LN, Becker AE. Functional and morphological organization of the rabbit sinus node. *Circ Res*. 1980;46:11–22.
16. Kodama I, Boyett MR. Regional differences in the electrical activity of the rabbit sinus node. *Pflugers Arch*. 1985;404:214–226.
17. Boyett MR, Honjo H, Kodama I. The sinoatrial node, a heterogeneous pacemaker structure. *Cardiovasc Res*. 2000;47:658–687.
18. James TN. Anatomy of the human sinus node. *Anat Rec*. 1961;141:109–139.
19. Honjo H, Boyett MR, Coppen SR, Takagishi Y, Opthof T, Severs NJ, Kodama I. Heterogeneous expression of connexins in rabbit sinoatrial node cells: correlation between connexin isotype and cell size. *Cardiovasc Res*. 2002;53:89–96.
20. Bleeker WK, Mackaay AJC, Masson-Pevet M, Op't Hof T, Jongsma HJ, Bouman LN. Asymmetry of the sino-atrial conduction in the rabbit heart. *J Mol Cell Cardiol*. 1982;14:633–643.
21. Schuessler RB, Boineau JP, Bromberg BI. Origin of the sinus impulse. *J Cardiovasc Electrophysiol*. 1996;7:263–274.
22. Betts TR, Ho SY, Sanchez-Quintana D, Roberts PR, Anderson RH, Morgan JM. Three-dimensional mapping of right atrial activation during sinus rhythm and its relationship to endocardial architecture. *J Cardiovasc Electrophysiol*. 2002;13:1152–1159.
23. Sanchez-Quintana D, Anderson RH, Cabrera JA, Climent V, Martin R, Farre J, Ho SY. The terminal crest: morphological features relevant to electrophysiology. *Heart*. 2002;88:406–411.